chemistry

MDPI

Article

Synthesis of Silver Nanocluster-Loaded FAU Zeolites and the Application in Light Emitting Diode

Tianning Zheng *, Ruihao Huang, Haoran Zhang, Song Ye * and Deping Wang

School of Materials Science and Engineering, Tongji University, Shanghai 201804, China; 2232898@tongji.edu.cn (R.H.); 2232891@tongji.edu.cn (H.Z.); wdpshk@tongji.edu.cn (D.W.)
* Correspondence: 2141994@tongji.edu.cn (T.Z.); yesong@tongji.edu.cn (S.Y.)

Abstract: Silver nanoclusters that are confined inside zeolites can give off intensive tunable emission across the visible region under UV excitation. In this research, a series of silver nanoclusters loaded with R-FAU/Ag (R = Li, Na, K) zeolites were synthesized and then applied as phosphors for LEDs. The XRD and SEM measurements showed the R-FAU/Ag (R = Li, Na, K) zeolites have high crystallinity and a size distribution of 0.7–1.25 μm. Under excitations of 310–330 nm ultraviolet radiation, Li-FAU/Ag, Na-FAU/Ag, and K-FAU/Ag exhibit monotonically declining emission intensities and red-shifted emissions with peak wavelengths of 520, 527, and 535 nm, respectively. By using silicone-based epoxy resin as the packaging material, a series of LEDs were fabricated by mixing R-FAU/Ag (R = Li, Na, K) phosphors. It is indicated that the Li-FAU/Ag-LED shows the strongest intensity of 94.9 mcd, much higher than that of the LEDs made from Na-FAU/Ag (63.7 mcd) and K-FAU/Ag (74.2 mcd) phosphors. Additionally, the chromaticity coordinate of the Li-FAU/Ag-LED is located at (0.2651, 0.4073) and has a high color temperature of 7873 K. Thermal test data showed that upon heating to 440 K, the intensities of R-FAU/Ag (R = Li, Na, K) LEDs decreased to 81%, 79%, and 75% of their initial intensities measured at 280 K, respectively. This research proposes a method for regulating the luminescent properties of silver nanoclusters in FAU zeolite by modifying the extra-framework cations and demonstrates excellent performance in LED products.

Keywords: FAU zeolite; silver nanocluster; luminescence property; LED; thermal stability

check for updates

Academic Editor: Iain A. Wright

Received: 25 April 2025
Revised: 22 May 2025
Accepted: 27 May 2025
Published: 30 May 2025

Citation: Zheng, T.; Huang, R.; Zhang, H.; Ye, S.; Wang, D. Synthesis of Silver Nanocluster-Loaded FAU Zeolites and the Application in Light Emitting Diode. *Chemistry* **2025**, *7*, 90. https://doi.org/10.3390/chemistry7030090

Copyright: © 2025 by the authors. Licensee MDPI, Basel, Switzerland. This article is an open access article distributed under the terms and conditions of the Creative Commons Attribution (CC BY) license (https://creativecommons.org/licenses/by/4.0/).

1. Introduction

As an emerging class of nanomaterials, silver nanoclusters have attracted considerable attention in imaging, detecting, optoelectronic, and lighting application fields due to their unique optical properties like high quantum yield approaching commercial phosphors and tunable emission in the visible to infrared regions [1–4]. The high surface energy of silver nanoclusters causes them to aggregate into larger silver nanoparticles with surface plasmon resonance (SPR) properties, which in turn leads to the quenching of their luminescence. To enable silver nanoclusters to emit bright light, appropriate matrices are needed. These matrices should not only prevent the excessive growth of silver clusters but also provide suitable crystal fields and site symmetries to maintain their optical activity [5–9].

Zeolites are microporous aluminosilicate crystals with well-defined quantum-sized pores, high cation exchange capacity, good stability, as well as high transparency in the visible light range, which have been considered ideal hosts to encapsulate luminescent guests like quantum dots, metal clusters, and nanocrystals [10–12]. Recent studies have indicated that the FAU, LTA, and SOD zeolites are desirable scaffolds for luminescent silver

nanoclusters [13–16]. The ability of zeolites to enable silver nanoclusters with highly efficient and tunable emission properties is not only due to their molecular-scale cage that can prevent over-aggregation but also their excellent ion exchange properties for the effective intake of silver ions. The framework structure of zeolites is composed of silicon–oxygen tetrahedra $[SiO_4]^{4-}$ and aluminum–oxygen tetrahedra $[AlO_4]^{5-}$. The framework as a whole is negatively charged due to the presence of $[AlO_4]^{5-}$, and therefore, the extra-framework cations, like sodium ions (Na^+), potassium ions (K^+), and lithium ions (Li^+), are required to make the charge balance. It was reported that the luminescence properties including emission wavelength and the intensity of the silver nanoclusters can be manipulated by adjusting the extra-framework cations of the host zeolite [17–19].

Some scholars have proposed that the silver nanocluster-loaded zeolites also show great potential in the development of chemical and biological sensors. This is because they possess high stability and unique luminescence performance. These materials can detect metal ions such as mercury ions (Hg^{2+}) and copper ions (Cu^{2+}), gas molecules such as oxygen (O_2) and carbon dioxide (CO_2), and biomolecules like glucose and uric acid with high sensitivity and high selectivity, demonstrating their important application prospect in the fields of environmental monitoring and medical diagnosis. For example, the luminescence behavior of silver nanoclusters in the zeolite matrix shows significant response to environmental stimuli. By regulating the pore size and surface chemical properties of the zeolite, the detection sensitivity and response speed can be further optimized [20–25]. In anti-counterfeiting technology, silver-exchanged zeolite LTA microcarriers are used to create high-resolution optical codes, such as quick response (QR) codes, via two-photon activation. The bright and stable emission of the silver nanoclusters ensures secure authentication, making it difficult to replicate. These microcarriers can be embedded in products like drugs and banknotes to serve as built-in security labels, enhancing product authenticity and preventing counterfeiting [26].

In addition, by adjusting the loading amount of Ag^+ and the heat treatment conditions, tunable emission and white light emission have been achieved by using FAU, LTA, and SOD zeolites as hosts, which makes the silver nanocluster-loaded luminescent zeolites attractive candidates for light-emitting diode (LED) applications. Researchers have recently discovered that when fabricated into white LED devices, using a UV-chip-on-board (UV-COB) chip, different excitation wavelengths cause LEDs to exhibit different optical properties. Using a 380 nm LED excitation, the Commission internationale de l'éclairage (CIE) color coordinate is (0.3207, 0.3575), the correlated color temperature (CCT) is 5986 K, the color rendering index—general (Ra) is 92.3, and color rendering index for red (R9) is 62. When using a 395 nm excitation LED, the CIE color coordinate is (0.3067, 0.3372), the CCT is 6757 K, the Ra is 94.9, and the R9 is 73. These parameters indicate that silver nanocluster-loaded luminescent zeolites can provide high-quality white light in LED applications, highlighting their potential as excellent materials for LED manufacturing [27–29]. Moreover, the emission properties of Li-LTA zeolites can be significantly tuned by dehydration, and the emission color can be tuned from blue to red. Notably, when excited at 340 nm, the Li-LTA zeolites emit bright green light and achieve an external quantum efficiency (EQE) of 83% [30]. Reported studies show that integrating luminescent silver nanoclusters into a conductive polymer matrix yields LEDs with tunable emission from blue to near-white. By adjusting the initial silver-loading degree in zeolites, this color-tuning can be achieved. Moreover, doping SOD zeolites with Ag^+, Eu^{3+}, and Zn^{2+} while using Eu^{3+} to promote silver nanocluster formation produces a broad emission spectrum ideal for white LEDs, offering a novel way to develop white-light-emitting devices [31]. The above research demonstrated the potential of zeolite-encapsulated silver nanoclusters for high-quality, tunable, and efficient lighting solutions.

In this study, a series of luminescent FAU zeolites loaded with silver nanoclusters and featuring different extra-framework cations (Li^+, Na^+, K^+) were prepared through ion exchange and heat treatment methods. Their structures, morphologies, and spectral properties were characterized by X-ray diffraction (XRD), X-ray photoelectron spectroscopy (XPS), scanning electron microscopy (SEM), and excitation–emission spectroscopy. These luminescent R-FAU/Ag (R = Li, Na, K) zeolites were used as phosphors, mixed with silicone-based epoxy resin, and fabricated into a series of LEDs go through a succession of encapsulation processes like vacuum degassing and high-temperature curing. The optical properties of the LED devices were tested using optical instruments, and appropriate mixing ratios and process flows were identified, ensuring that the LED devices possess excellent photoelectric characteristics and high-temperature stability superior to that of commercial light sources.

2. Materials and Methods

2.1. Materials

The raw materials, including $NaAlO_2$ (analytic purity), NaOH (analytic purity), $Na_2SiO_3{\cdot}9H_2O$ (analytic purity), $LiNO_3$ (99.99%, metals basis), and $AgNO_3$ (99.8%), were all purchased from Aladdin Chemical Co., Ltd. (Shanghai, China), which were used without further purification. Type A and type B silicone-based epoxy resin (type: PNS 30360 A&B) were purchased from Protavic International Chemical Co., (Levallois-Perret, France). The UV chip uses the model 3535 UVC from leienda opto-electronics company (Shenzhen, China).

2.2. Synthesis of R-FAU (R = Li, Na, K) Zeolite

In the synthesis of Na-FAU zeolite, two equal sets of 0.64 g NaOH were firstly weighted and dissolved in 50 mL deionized water, and then 22.736 g $Na_2SiO_3{\cdot}9H_2O$ and 4.684 g $NaAlO_2$ were, respectively, added into NaOH solution and mixed. The mixture stood for 24 h before reacting at 120 °C for 3 h in a polytetrafluoroethylene vessel. Finally, the slurry was centrifuged, washed with deionized water, and dried overnight at 80 °C to obtain the phosphor Na-FAU zeolite, named Na-FAU.

Each 1 g of the above Na-FAU zeolite was suspended in 50 mL $LiNO_3$ or KNO_3 aqueous solution with concentration of 5.0 mol/L. The above suspensions were kept stirring at 80 °C for 12 h and then washed with deionized water before dried at 80 °C for 24 h. The final product was named R-FAU (R = Li, Na, K) [32,33].

2.3. Synthesis of Silver Clusters Loaded R-FAU (R = Li, Na, K) Zeolites

A total of 1 g of R-FAU (R = Li, Na, K) phosphor obtained in the previous step was mixed with 100 mL of $AgNO_3$ aqueous solution with concentration of 20.0 mmol/L. The mixture was shaken at room temperature for 8 h and then centrifuged, washed with deionized water, and dried overnight at 80 °C. After that, the obtained phosphor was annealed at 600 °C for 2 h in air. The final products were named as R-FAU/Ag (R = Li, Na, K) accordingly.

2.4. Fabrication of R-FAU/Ag (R = Li, Na, K) Phosphor-Based LED

To integrate R-FAU/Ag (R = Li, Na, K) phosphors into LED devices, the process involves several of the following key steps: phosphors and silicone-based epoxy resin mixing, encapsulation, defoaming, coating, and curing.

Firstly, place type A and type B silicone-based epoxy resin together with each of the R-FAU/Ag (R = Li, Na, K) phosphors into a beaker. The type A and type B silicone-based epoxy resin should be in a ratio of 1:1, with 10 g for each type. The ratio of the phosphors to

the silicone-based epoxy resin should be added in a range from 1:8 to 1:16; put the long-arm stirrer into the beaker and stir with a mixer at a speed of 80 rad/min for 15 min to ensure the phosphor is uniformly dispersed in the silicone-based epoxy resin. Then, transfer the beaker into a vacuum defoaming machine, set the vacuum pressure value to less than 0.08 MPa and the defoaming time to 5 min. After that, during the dispensing and coating process, load the defoamed colloid into a dispensing needle. Set the dispensing amount to 2 mg and the dispensing time to 0.5 s. Then, evenly coat the mixture onto the surface of the ultraviolet light-emitting diode (UV LED) chip. Finally, fix the coated chip on a bracket and place it in a high-temperature oven for curing. The curing process was performed at 85 °C for 2 h. The obtained LEDs were named R-FAU/Ag-LEDs (R = Li, Na, K) accordingly.

2.5. Measurement

The XRD patterns of the samples were recorded on Rigaku Smartlab9 (Tokyo, Japan) diffractometer with Cu-Kα radiation (λ = 1.5406 Å, Scanning rate = 5°/min at 40 KV and 20 mA). The scanning electron microscopy (SEM) and energy dispersive X-ray diffraction (EDX) measurements were carried out on ZEISS Gemini 300 (Jena, Germany). The photoluminescence (PL) and the photoluminescence of excitation (PLE) spectra were recorded with Edinburgh FLS980 (Livingston, UK). The X-ray photoelectron spectroscopy (XPS) measurements were carried out on the Thermo ESCALAB 250XI (Waltham, MA, USA) by using AlKα X (hυ = 1486.6 eV, 650 μm of beam spot) as the incident radiation source. The optical spectrum and light intensity tests of the LED devices were conducted using the HPCS6300 equipment from HOPOOColor (Hangzhou, China). The thermal stability experiment of the LED devices was evaluated using a high–low temperature test chamber NDSD-415T manufactured by Nobede (Shenzhen, China). The surface temperature of the LED was monitored by a thermocouple Omega HSTC-TT-K-20S-120 (Greenwich, CT, USA). The size and brightness of the light spot were measured using an imaging luminance meter LMK6-12 produced by TechnoTeam Bildverarbeitung GmbH (Berlin, Germany).

3. Results and Discussion

After the synthesis of R-FAU/Ag (R = Li, Na, K), XRD measurement was first carried out to determine whether the prepared zeolites are the target products and to study the impact of cation exchange on the crystal structure. The XRD patterns of the synthesized R-FAU/Ag (R = Li, Na, K) zeolites are shown in Figure 1. The main figure on the left shows the diffraction situation in the range of 2θ from 2° to 45°, capturing the main diffraction peaks of the crystal structures of R-FAU/Ag (R = Li, Na, K) zeolites. The enlarged patterns on the right provide a more detailed view of the diffraction peaks within 5.8°~6.5° and 22.5°~24.5° 2θ intervals. As can be seen from the main figure, the diffraction peaks of R-FAU/Ag (R = Li, Na, K) are highly consistent with the JCPDS# 43-0168 standard [34] card, indicating the successful synthesis of the zeolite. It can be observed from the enlarged patterns on the right that, compared with Na-FAU/Ag, the diffraction peaks of Li-FAU/Ag shift towards larger angles. This is because the ionic radius of Li^+ is smaller than that of Na^+. When Li^+ replaces Na^+, the lattice contracts, and the interplanar spacing (d) decreases, and the diffraction angle (θ) increases. Conversely, the diffraction peaks of K-FAU/Ag shift towards smaller angles because the ionic radius of K^+ is larger than that of Na^+, and the substitution of K^+ for Na^+ leads to lattice expansion. The above XRD results indicated that the Na-FAU zeolite was successfully synthesized, and the Li^+ and K^+ have replaced the positions of Na^+ during the afterward ion exchange processes [35,36].

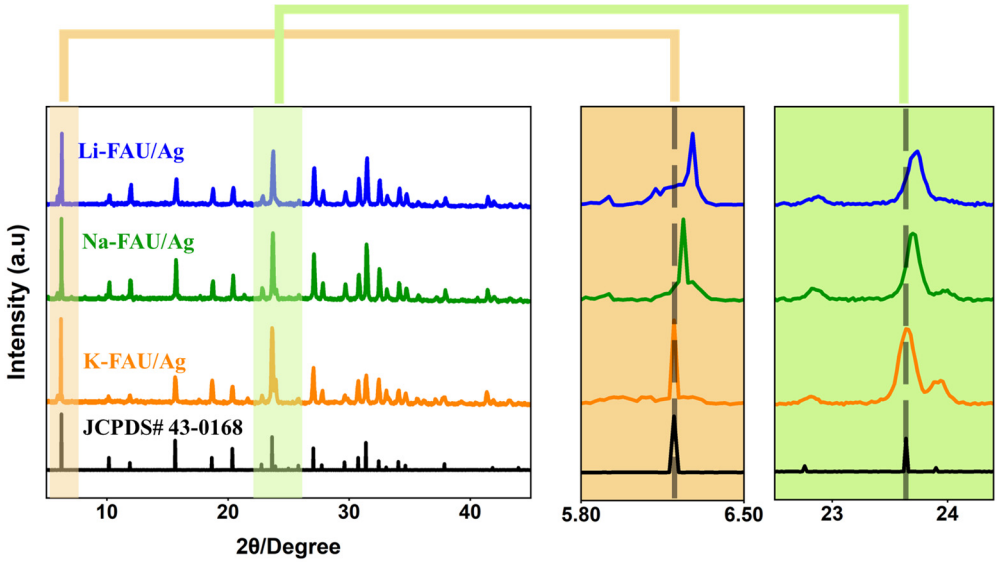


Figure 1. X-ray diffraction patterns of R-FAU/Ag (R = Li, Na, K), Peaks at 5.8–6.5° and 22.5–24.5° have been amplified.

In order to confirm the morphology and particle size of the R-FAU/Ag (R = Li, Na, K) zeolites and determine whether they were suitable as phosphor materials, SEM experiments were carried out to study the morphology and particle size. The SEM images show that the particles exhibited cubic or octahedral shapes with smooth surfaces and well-defined edges, indicating their high crystallinity, as shown in Figure 2(a1–c1). The statistical average particle sizes of Li-FAU/Ag, Na-FAU/Ag, and K-FAU/Ag were 0.85, 0.95, and 0.80 μm, which were in a similar range, as shown in Figure 2(a2–c2). A smooth surface can reduce the diffusion resistance and decrease the friction coefficient between the phosphor and the packaging material, which is beneficial to the diffusion of the phosphor in the LED encapsulating material, and a similar particle size range is beneficial for the consistency of the thickness of the phosphor layer, resulting in uniform light emission. These characteristics indicate that the R-FAU/Ag (R = Li, Na, K) particles are suitable for being used as phosphor materials for packaging.

Additionally, EDX analysis and elemental mapping were conducted to investigate the distribution of various elements. The EDX analysis and element mapping were performed on R-FAU/Ag (R = Li, Na, K), and the results are presented in Figure 3a–c. Through these analyses, oxygen (O), sodium (Na), potassium (K), aluminum (Al), silicon (Si), and silver (Ag) were all detected. From the elemental mapping images in the upper right corner, tall constituent elements are uniformly distributed. According to the elemental content, O has the highest content, accounting for 50.1% by weight. This indicates that O atoms are involved in constructing the basic skeletal structure. The ratio of Al to Si in R-FAU/Ag (R = Li, Na, K) is approximately 0.4, suggesting that the basic structures of the three zeolites are consistent. Although Li was not detected due to its low energy, the content of Na was detected in the Li-FAU/Ag and Na-FAU/Ag samples. It was found that the weight percentage of the Na element in Li-FAU/Ag is 55% less than that in Na-FAU/Ag, and no other elements were detected in the samples, indicating that Li had successfully replaced some of the Na elements. At the same time, the Ag element was detected in all three zeolites, with a weight percentage of 12%. This indicates that the zeolites have successfully undergone Ag exchange. The results of the elemental analysis by EDX indicate that the prepared particles already conform to the characteristics of R-FAU/Ag (R = Li, Na, K), and all the constituent elements are evenly distributed.

The XPS survey spectra of R-FAU/Ag (R = Li, Na, K) are presented in Figure 4a, from which the peak of Na 1s can be clearly seen for Na-FAU/Ag. For Li-FAU/Ag and K-FAU/Ag, the peaks of Li 1s and K 2p can be observed, respectively, while that of Na 1s has almost disappeared. These XPS results indicate that Li^+ and K^+ successfully replaced Na^+ during the ion exchange process [33]. Moreover, in order to further identify the chemical state of the silver, species formed inside the R-FAU/Ag (R = Li, Na, K) zeolites with different extra-framework cations, and the XPS high-resolution energy spectra of Ag 3d were measured and shown in Figure 4b, and the two photoelectron peaks with a large difference in binding energy can be well attributed to Ag $3d_{3/2}$ and Ag $3d_{5/2}$, respectively. The binding energies of Ag $3d_{3/2}$ and Ag $3d_{5/2}$ are around 374.6 and 368.7 eV for R-FAU/Ag (R = Li, Na, K), which fall in the binding energy range of Ag for silver nanoclusters [37–39].

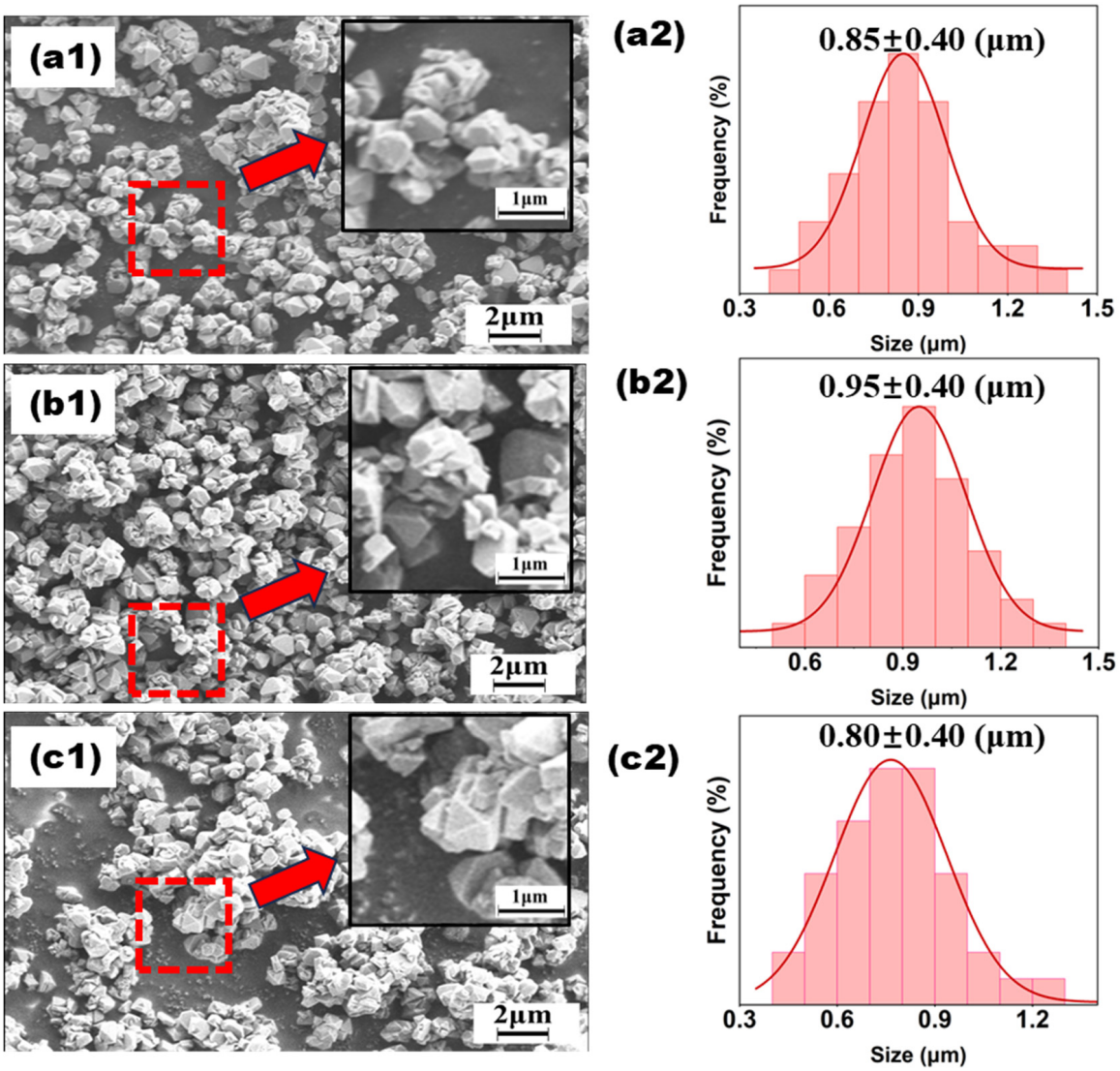


Figure 2. Scanning electron microscopy and particle size statistics of Li-FAU/Ag (**a1**,**a2**), Na-FAU/Ag (**b1**,**b2**), and K-FAU/Ag (**c1**,**c2**).

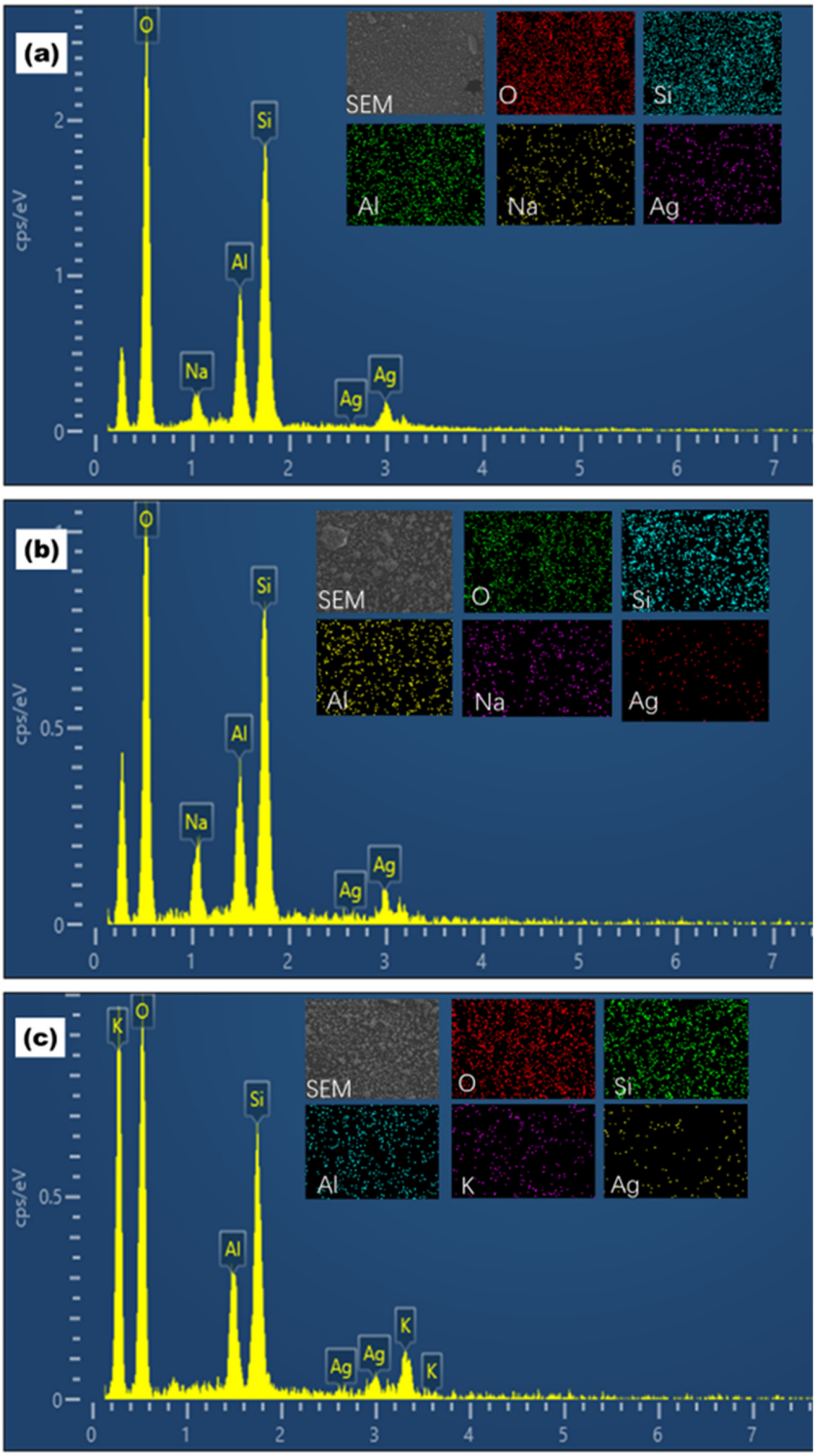


Figure 3. The element mapping of Li-FAU/Ag (**a**), Na-FAU/Ag (**b**), and K-FAU/Ag (**c**).

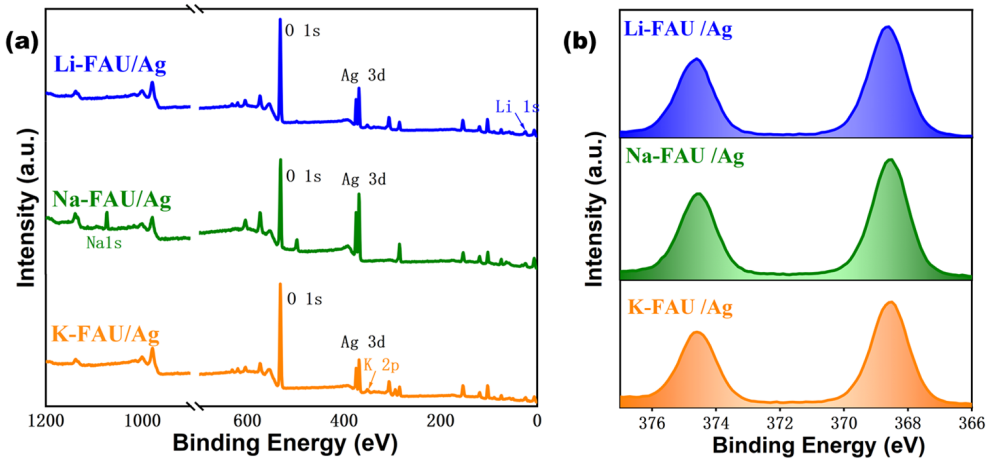


Figure 4. XPS survey spectra (**a**) and high-resolution spectra of Ag (**b**) for R-FAU/Ag (R = Li, Na, K).

Figure 5 shows the PLE and PL spectra of R-FAU/Ag (R = Li, Na, K) phosphor. As can be observed, the excitation peaks are located at 312, 326, and 330 nm, respectively, for Li-FAU/Ag, Na-FAU/Ag, and K-FAU/Ag, indicating these silver nanoclusters that are confined inside FAU zeolites can be effectively excited by UV light. Under the most efficient excitation of each sample, the emission peak of silver nanoclusters varies, which is located at around 520 nm in Li-FAU/Ag, and then, red shifted to 527 nm in Na-FAU/Ag and further to 535 nm in K-FAU/Ag. According to previous studies, the Ag_3^{n+} clusters generated at the double six-ring (D6r) cages of FAU zeolites after thermal treatment are responsible for the high luminescent green emission under UV excitation [40,41]. It is also noticed that the emission intensity of the silver clusters is also greatly influenced by the host zeolite, Li-FAU/Ag exhibits the strongest emission while K-FAU/Ag shows the weakest emission. This extra-framework dependence on the luminescence properties of silver nanoclusters is in accordance with the previous reports [15,42,43].

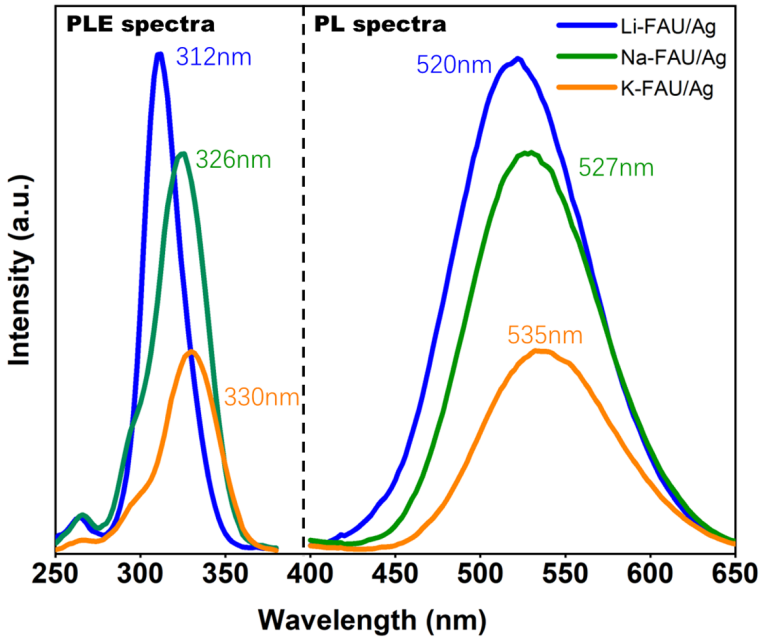


Figure 5. PLE and PL spectra of R-FAU/Ag (R = Li, Na, K).

Based on the most emission-efficient Li-FAU/Ag phosphor, the Li-FAU/Ag-LEDs were successfully prepared. Figure 6a shows the states of mixtures with different ratios of phosphor to silicone-based epoxy resin. The phosphor concentration of the left sample is

relatively as low as 6.2%, and it gradually increases to 12.5% towards the right. It can be observed that when the phosphor concentration is low, the mixture remains clear, while it gradually becomes turbid as the concentration increases. Figure 6b shows the states of LEDs prepared with different Li-FAU/Ag phosphor to silicone-based epoxy resin ratios. It can be seen that when the phosphor concentration is low, the UV LED chip is visible, just like the first LED on the left. And as the phosphor concentration increases to 7.1%, the chip becomes invisible. When the concentration exceeds 7.1%, the phosphor layer gradually darkens, and at concentrations above 10%, it appears completely black. Figure 6c illustrates the emission states of Li-FAU/Ag-LEDs with different phosphor to silicone-based epoxy resin ratios with ninepowered with the same voltage and current (5.3 V, 150 mA), lighting a white resin board. The results show that at a phosphor concentration of 6.3%, the emitted light is dim and blue. The light spot has a diameter of 6.2 mm and a brightness of 35.41 cd/m^2, measured by an imaging luminance meter. We speculate that at low phosphor concentrations, the limited number of phosphor particles cannot fully convert UV light. Unconverted UV light near the visible spectrum appears as blue light after scattering, forming a blue spot. Also, fewer particles lead to less light scattering, resulting in a smaller spot. As the phosphor concentration rises, the spot diameter increases, and its color shifts from blue to white. The brightest spot occurs at 7.1% phosphor concentration, with a diameter of 18.3 mm and brightness of 68.20 cd/m^2, indicating the highest conversion efficiency. Continuously increasing the content of the phosphor, the size of the light spot remains almost unchanged, but the brightness gradually dims. At 11.1% concentration, the brightness approaches nearly 0 cd/m^2. This means extra phosphors beyond this point do not improve conversion and instead block visible light transmission. Table 1 shows the lighting parameters for each concentration of the Li-FAU/Ag phosphor.

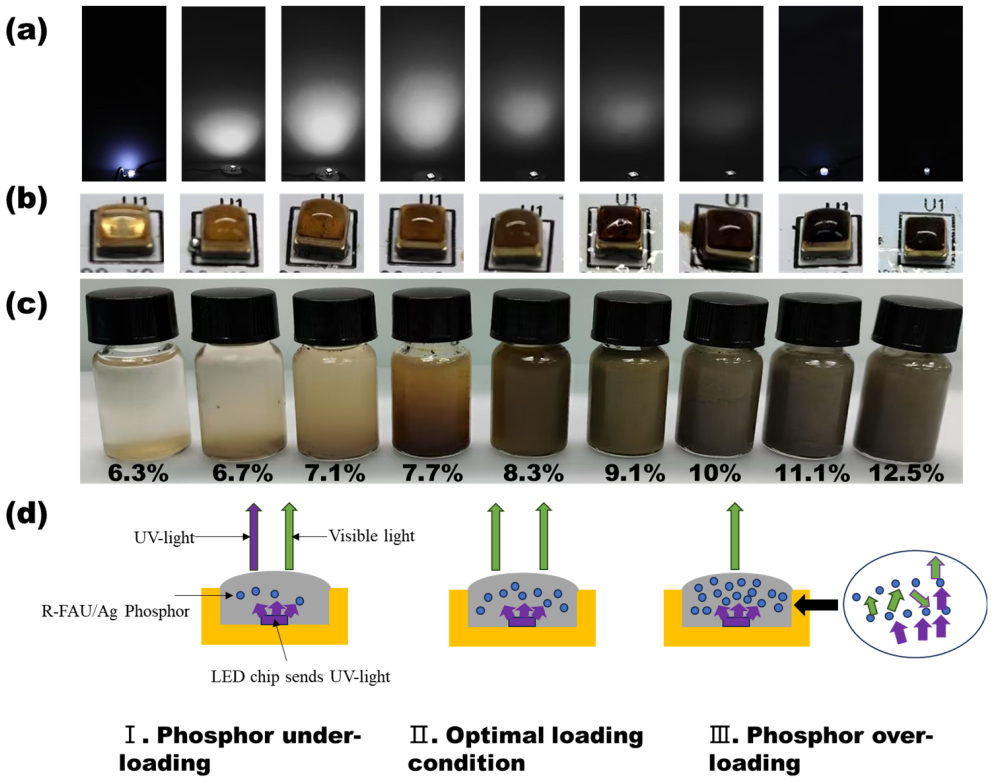


Figure 6. Silicone-based epoxy resin state after mixing with different amounts of Li-FAU/Ag phosphor; (**a**) turbidity of the phosphor-containing glue at different mixing concentrations. (**b**) Appearance of the LEDs fabricated at different mixing concentrations. (**c**) Fabricated LEDs lighting a whiteboard under working conditions. (**d**) Illustration of the influence of phosphor content on light extraction.

Table 1. Different Li-FAU/Ag concentration VS lighting parameter.

Concentration	6.3%	6.7%	7.1%	7.7%	8.3%	9.1%	10%	11.1%	12.5%
Brightness (cd/m^2)	35.41	56.4	68.20	57.77	48.81	32.48	5.62	0.48	0.21
Light spot diameter (mm)	6.2	16.2	18.3	18.1	17.7	16.4	15.7	6.2	4.3

The above experimental phenomena suggested that the ratio of R-FAU/Ag (R = Li, Na, K) phosphor to silicone-based epoxy resin significantly affects the light conversion efficiency of LEDs. When the proportion of the phosphor is too low, the ultraviolet light cannot be effectively absorbed, resulting in a decrease in the intensity of the emitted light (as shown in Figure 6d-I). Conversely, when the proportion of the phosphor is too high, it will lead to severe scattering and reabsorption of visible light within the phosphor layer, ultimately significantly reducing the output of visible light (as shown in Figure 6d-III). Under the ideal proportion of the phosphor (as shown in Figure 6d-II), the thickness of the phosphor layer is moderate, enabling it to fully absorb ultraviolet light and efficiently convert it into visible light while avoiding excessive scattering and reabsorption effects. Based on the above principles, it is evident that optimizing the proportion of the phosphor plays a crucial role in improving the light output efficiency of LEDs.

In this research, we further mixed R-FAU/Ag (R = Li, Na, K) with silicone-based epoxy resin in different ratios to fabricate a series of LED devices, and the optical performance of these devices was also evaluated. As shown in Figure 7a, the emission intensities of R-FAU/Ag (R = Li, Na, K) exhibit the same W_{powder}/W_{total} mixing ratio dependency under 325 nm UV chip excitation, which initially increases with the increase in mixing ratio and then rapidly decreases with a further enhanced mixing ratio. This trend is consistent with the observations in Figure 6, which verified the reliability of the experimental results. Furthermore, the optimal phosphor concentrations for maximizing the UV light conversion efficiency of the Li-FAU/Ag-LED, Na-FAU/Ag-LED, and K-FAU/Ag-LED were determined to be 7.1%, 7.7%, and 9%, respectively. Among these devices, the Li-FAU/Ag-LED exhibited the highest light extraction intensity, reaching 94.9 mcd.

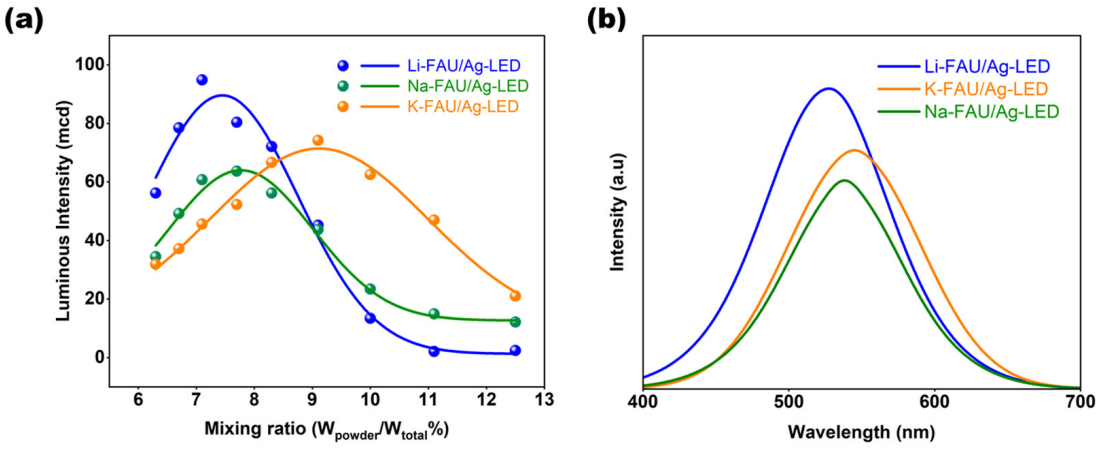


Figure 7. (**a**) Phosphor concentration dependence of LED luminous intensities and (**b**) visible spectra of R-FAU/Ag-LEDs (R = Li, Na, K).

The emission spectra of the UV LEDs fabricated according to the optimized ratio of phosphor to silicone-based epoxy resin are depicted in Figure 7b. When excited by a 325 nm UV chip, the R-FAU/Ag (R = Li, Na, K)-LEDs exhibit distinct emission peaks. Specifically, the Li-FAU/Ag-LED shows an emission peak at 527 nm, the Na-FAU/Ag-LED at 538 nm, and the K-FAU/Ag-LED at 545 nm. These emission peaks shift towards

longer wavelengths compared with the PLE and PL spectra of R-FAU/Ag (R = Li, Na, K) (Figure 5). We speculate that the wavelength of light changes when it propagates in media with different refractive indices. A medium with a higher refractive index makes the light wavelength appear longer. The refractive index of the silicone-based epoxy resin is 1.5, which causes the visible light converted by the phosphor to undergo a red shift after refraction.

We also used optical testing instruments (HOPOOColor) to evaluate the optical performance of these LEDs. Table 2 shows the optical performance parameters of R-FAU/Ag-LEDs (R = Li, Na, K), including thechromaticity coordinates x and y, color temperature, peak wavelength, luminous intensity, luminous efficacy, and conversion efficiency. As can be observed for the Li-FAU/Ag-LED, it has chromaticity coordinates of x = 0.2651 and y = 0.4073, with a relatively high color temperature of 7873 K. The emission peak wavelength is located at 527 nm, in the blue–green region. The luminous intensity reaches 94.9 mcd, the luminous efficacy is 19.7 lm/W, the conversion efficiency is the highest among the three samples at 59.3%, and the general color rendering index (Ra) is 46.5. The Na-FAU/Ag-LED has chromaticity coordinates of x = 0.2979 and y = 0.4666, with a color temperature of 6387 K, which is lower than that of the Li-FAU/Ag-LED. Its emission peak wavelength is 538 nm, longer than that of the Li-FAU/Ag-LED. The luminous intensity is 63.7 mcd, lower than the Li-FAU/Ag-LED, the luminous efficacy is 13.2 lm/W, and the conversion efficiency is 39.8%, which is the lowest among the three samples, and the Ra is 52.2. The K-FAU/Ag-LED has chromaticity coordinates of x = 0.3076 and y = 0.4893, with a color temperature of 6087 K, the lowest among the three samples. Its peak wavelength is 545 nm, the longest among the three. The luminous intensity is 74.2 mcd, and the luminous efficacy is 15.6 lm/W, with a conversion efficiency of 47%, ranking between the Li-FAU/Ag-LED and the Na-FAU/Ag-LED, and the Ra is 62.9, which is the highest among the three. The above data indicated that by adjusting the extra-framework cations of the R-FAU/Ag (R = Li, Na, K) zeolites, the color and luminous intensities of R-FAU/Ag-LEDs (R = Li, Na, K) devices can be well regulated. This is consistent with the previously reported phenomenon that changing the alkaline ions can alter the emission luminous intensities and color of silver nanoclusters [33]. The optical performance of the LED devices fits the experimental results very well. Meanwhile, the highest luminous efficacy is 19.7 lm/W for the Li-FAU/Ag-LED, which has met the lighting requirements of general commercial LEDs. In some specific application scenarios, such as those that require both UV lighting and general lighting, it can exert its special properties. As shown in Figure 8, the chromaticity coordinates of R-FAU/Ag-LEDs (R = Li, Na, K) are plotted in the CIE 1931 chromaticity diagram [44].

Table 2. R-FAU/Ag-LEDs (R = Li, Na, K) optical performance.

Parameter	*x*	*y*	Color Temperature	Peak Wavelength	Intensity	Efficacy	Conversion Efficiency	Ra
			K	nm	mcd	lm/W		
Li-FAU/Ag-LED	0.2651	0.4073	7873	527	94.9	19.7	59.30%	46.5
Na-FAU/Ag-LED	0.2979	0.4666	6387	538	63.7	13.2	39.80%	52.2
K-FAU/Ag-LED	0.3076	0.4893	6087	545	74.2	15.6	47%	62.9

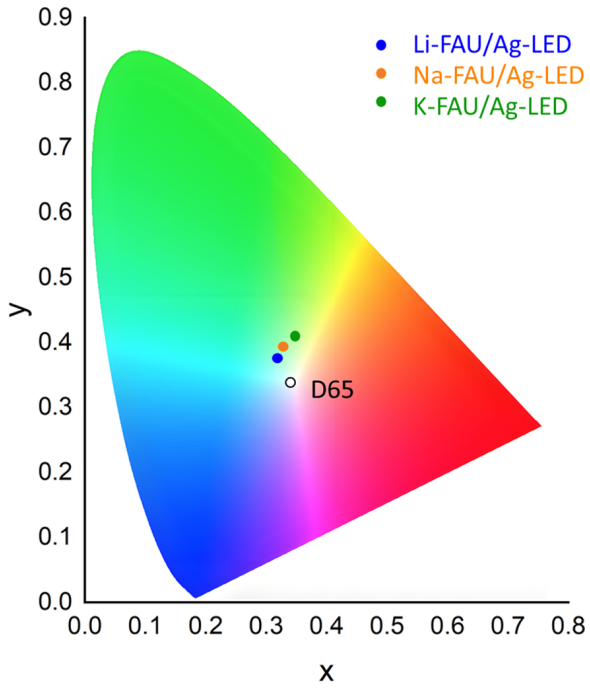


Figure 8. CIE chromaticity diagram of R-FAU/Ag-LED (R = Li, Na, K).

In addition, a series of thermal stability tests were conducted to evaluate the practical applicability of the synthesized LEDs. By measuring the luminous intensity changes of R-FAU/Ag-LEDs (R = Li, Na, K) at different temperatures, we can directly assess their luminous intensity attenuation performance in actual high-temperature working environments. The temperature dependence of emission spectra and integrated emission intensities for the R-FAU/Ag-LED (R= Li, Na, K) are shown in Figure 9, which clearly illustrates the luminous intensity changes of R-FAU/Ag-LEDs (R = Li, Na, K) under high temperatures up to 440 K. Initially, at a room temperature of 280 K, all three samples of R-FAU/Ag-LEDs (R = Li, Na, K) exhibit their respective maximum luminous intensity. At 440 K, the luminous intensities of the Li-FAU/Ag-LED, Na-FAU/Ag-LED, and K-FAU/Ag-LED decrease to 81%, 79%, and 75% of their respective values at room temperature. Meanwhile, we also recorded the change in temperature over time when the LEDs were lit at different temperatures. As shown in the middle diagram of Figure 9, it can be observed that the brightness decreases rapidly within the first 30 min and tends to stabilize after 30 min. We speculate that an increase in temperature can cause an increase in the concentration of electrons and holes inside a UV LED, a reduction in the band gap, and a decrease in electron mobility. As a result, the probability of radiative recombination of electrons and holes in the potential decreases, while non-radiative recombination occurs, generating heat from the UV chip, reducing the internal quantum efficiency and causing a decrease in the intensity of the UV light [45].

To gain a more comprehensive understanding of the temperature dependence of luminescence properties, we compared the thermal stability of the prepared R-FAU/Ag-LEDs (R = Li, Na, K) with that of commercial LEDs. Conventional commercial LEDs often face significant challenges in maintaining stable luminous intensities under high-temperature conditions. The luminous intensities of some commonly used commercial LEDs decrease more significantly, and at 440 K, their luminous intensities drop below 70% of their values at room temperature [46]. In contrast, the Li-FAU/Ag-LED retains 81% of its initial luminous intensities, demonstrating relatively excellent thermal stability. The Na-FAU/Ag-LED also performs well, retaining 79% of its initial luminous intensities. Even the K-FAU/Ag-LED, although having the lowest retention rate of 75% among our samples, still shows comparable

performance to some conventional commercial LEDs. We speculate that it is because the UV light does not contain infrared rays, which reduces the temperature rise of the irradiated silicone-based epoxy resin. Moreover, our UV chips are packaged with copper brackets, which is conducive to faster heat dissipation. In contrast, commercial LEDs use plastic brackets, and their thermal conductivity is too low. This is why R-FAU/Ag-LEDs (R = Li, Na, K) exhibit better heat resistance than commercial LEDs.

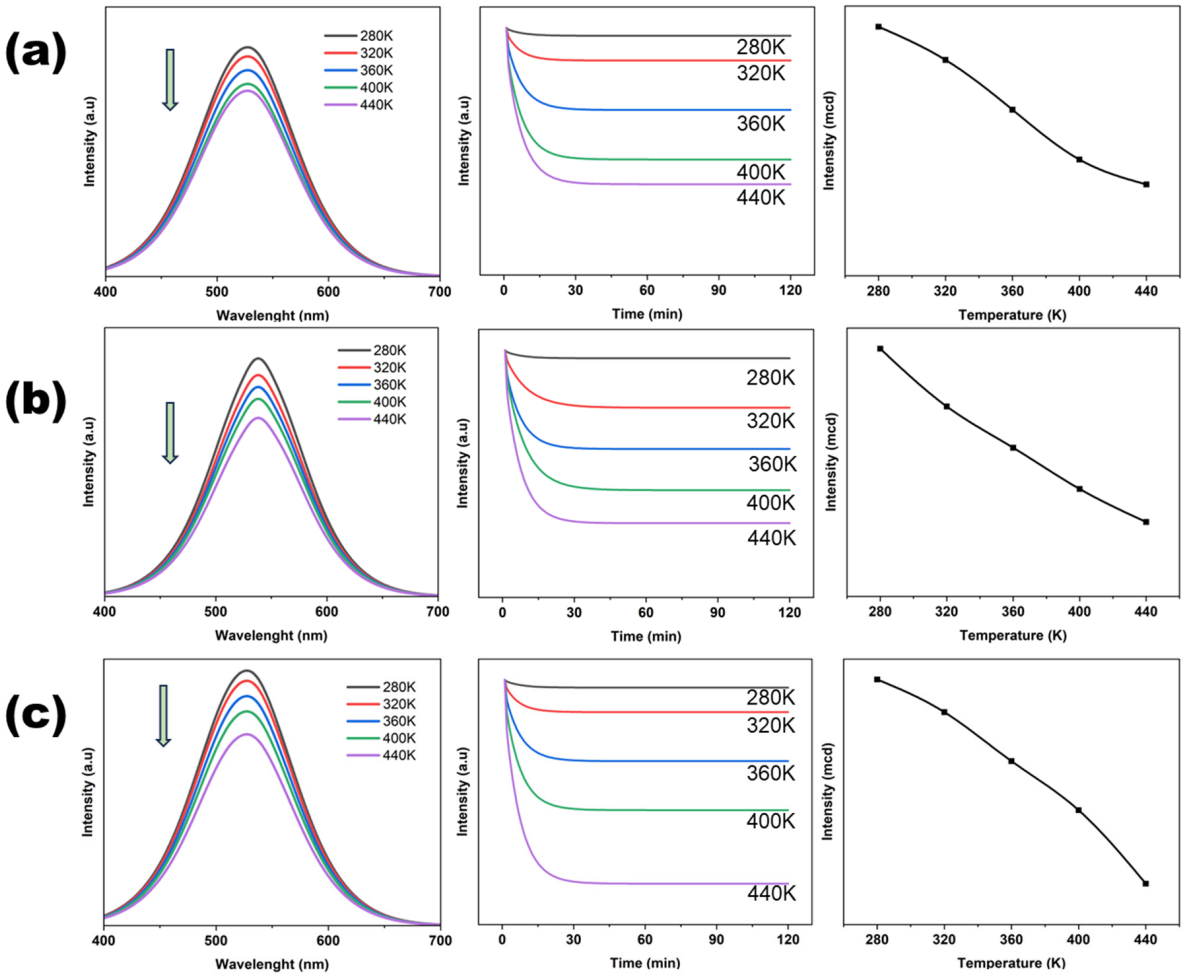


Figure 9. Temperature dependence of intensities for (**a**) Li-FAU/Ag-LED, (**b**) Na-FAU/Ag-LED, and (**c**) K-FAU/Ag-LED.

Furthermore, the reason why the decreasing proportions of the luminous intensities of the three samples are different is that optimal phosphor concentrations of R-FAU/Ag-LEDs (R = Li, Na, K) are different, and the amounts of phosphors used also vary. Since the phosphor has low thermal conductivity, it will also reflect a part of the UV light back into the LED chip; the more phosphor is used, the more likely heat will accumulate inside the LED, and the faster the luminous intensities will decrease. At the optimal ratio, the content of the Li-FAU/Ag-LED phosphor is 7.1%, which is the lowest amount of phosphor, and the luminous intensities decrease is also the lowest. In contrast, the content of the K-FAU/Ag-LED phosphor is 9%, and the luminous intensities decrease is the highest. This is consistent with the trend shown in Figure 9.

4. Conclusions

In this study, R-FAU/Ag (R = Li, Na, K) zeolites were synthesized using hydrothermal and ion exchange methods and used as host materials for silver nanocrystals. Under

ultraviolet excitation, the solid-state silver nanoclusters that were confined inside FAU zeolites with extra-framework cations of Li^+, Na^+, and K^+ exhibited red-shifted emission and reduced intensity in the visible region. These luminescent zeolites were further used as phosphors together with silicone-based epoxy resin to fabricate a series of light-emitting diodes (LEDs). The optimal mixing ratios of Li-FAU/Ag, Na-FAU/Ag, and K-FAU/Ag were determined to be 7.1%, 7.7%, and 9%, respectively. Appropriate ratios improved the light output efficiency of the LEDs. Under 325 nm excitation, the Li-FAU/Ag with an emission peak wavelength of 527 nm showed a luminous efficiency of 19.7 lm/W and a conversion efficiency of 59.30%. At 440 K, the luminous intensities of R-FAU/Ag-LEDs (R = Li, Na, K) were 81%, 79%, and 75% of their room temperature values, respectively. The Li-FAU/Ag-LED exhibited the highest light intensity (94.9 mcd), outperforming the Na-FAU/Ag-LED (63.7 mcd) and the K-FAU/Ag-LED (74.2 mcd). The luminescent zeolite-based LEDs fabricated in this study demonstrate excellent optical properties, high luminous efficiency, and good high-temperature characteristics, holding broad application prospects in the field of LED applications.

Author Contributions: Conceptualization, T.Z.; methodology, S.Y.; validation, D.W. and R.H.; data curation, H.Z.; writing—original draft preparation, T.Z.; writing—review and editing, S.Y. All authors have read and agreed to the published version of the manuscript.

Funding: This work was financially supported by the National Natural Science Foundation of China (Nos. 51872200, 51772210) and the Natural Science Foundation of Shanghai (No. 18ZR1441900).

Data Availability Statement: The original contributions presented in this study are included in this article, and further inquiries can be directed to the corresponding authors.

Conflicts of Interest: The authors declare no conflicts of interest.

References

1. Devaraj, V.; Lee, I.H.; Kim, M.; Nguyen, T.M.; Son, J.P.; Lee, J.-M.; Lee, D.; Kim, K.H.; Oh, J.-W. Unveiling facet effects in metallic nanoparticles to design an efficient plasmonic nanostructure. *Curr. Appl. Phys.* **2022**, *44*, 22–28. [CrossRef]
2. Evstropiev, S.K.; Nikonorov, N.V.; Saratovskii, A.S. Double stabilization of silver molecular clusters in thin films. *Res. Chem. Intermed.* **2020**, *46*, 4033–4046. [CrossRef]
3. Xie, Y.P.; Shen, Y.L.; Duan, G.X.; Han, J.; Zhang, L.P.; Lu, X. Silver nanoclusters: Synthesis, structures and photoluminescence. *Mater. Chem. Front.* **2020**, *4*, 2205–2222. [CrossRef]
4. Jonckheere, D.; Coutino-Gonzalez, E.; Baekelant, W.; Bueken, B.; Reinsch, H.; Stassen, I.; Fenwick, O.; Richard, F.; Samorì, P.; Ameloot, R.; et al. Silver-induced reconstruction of an adeninate-based metal–organic framework for encapsulation of luminescent adenine-stabilized silver clusters. *J. Mater. Chem. C* **2016**, *4*, 4259–4268. [CrossRef]
5. Quintanilla, M.; Liz-Marzan, L.M. Caged clusters shine brighter. *Science* **2018**, *361*, 645. [CrossRef]
6. Diez, I.; Ras, R.H. Fluorescent silver nanoclusters. *Nanoscale* **2011**, *3*, 1963–1970. [CrossRef]
7. Romolini, G.; Steele, J.A.; Hofkens, J.; Roeffaers, M.B.J.; Coutino-Gonzalez, E. Tunable Luminescence from Stable Silver Nanoclusters Confined in Microporous Zeolites. *Adv. Opt. Mater.* **2021**, *9*, 2100527. [CrossRef]
8. De Cremer, G.; Coutiño-Gonzalez, E.; Roeffaers, M.B.J.; Moens, B.; Ollevier, J.; Schoonheydt, R.; Jacobs, P.A.; De Schryver, F.C.; Hofkens, J.; De Vos, D.E.; et al. Characterization of fluorescence in heat-treated silver-exchanged zeolites. *J. Am. Chem. Soc.* **2009**, *131*, 3049–3056. [CrossRef]
9. Aono, H.; Yahara, K.; Johan, E.; Itagaki, Y. Effect of coexisting lithium content on fluorescent properties of silver ion-exchanged LTA zeolite. *J. Ceram. Soc. Jpn.* **2020**, *128*, 670–676. [CrossRef]
10. Ahmad, I.; Muhmood, T.; Rehman, A.; Zahid, M.; Abohashrh, M.; Nishat, S.; Raharjo, Y.; Zhou, Z.; Yang, X. Zeolite imidazole framework entrapped quantum dots (QDs@ ZIF-8): Encapsulation, properties, and applications. *J. Taiwan. Inst. Chem. Eng.* **2023**, *149*, 104993. [CrossRef]
11. Coutino-Gonzalez, E.; Baekelant, W.; Grandjean, D.; Roeffaers, M.B.J.; Fron, E.; Aghakhani, M.S.; Bovet, N.; Van der Auweraer, M.; Lievens, P.; Vosch, T.; et al. Thermally Activated LTA (Li)-Ag Zeolites with Water-Responsive Photoluminescence Properties. *J. Mater. Chem. C* **2015**, *3*, 11857–11867. [CrossRef]
12. Johan, E.; Kanda, Y.; Matsue, N.; Itagaki, Y.; Aono, H. Whitish fluorescence of partially Ag-exchanged zeolite Y affected by coexisting cations. *J. Lumin.* **2019**, *213*, 482–488. [CrossRef]

13. Li, Q.; Yuan, J.; Zhao, D.; Wang, Y.; Li, H. Stable and Highly Luminescent Silver Nanoclusters in the 13X Zeolite Enabled by Mg^{2+} Doping and Their Luminescence Tuning by Heating Temperature. *Inorg. Chem.* **2023**, *62*, 18299–18306. [CrossRef]
14. Grandjean, D.; Coutino-Gonzalez, E.; Cuong, N.T.; Fron, E.; Baekelant, W.; Aghakhani, S.; Schlexer, P.; D'Acapito, F.; Banerjee, D.; Roeffaers, M.B.J.; et al. Origin of the bright photoluminescence of few-atom silver clusters confined in LTA zeolites. *Science* **2018**, *361*, 686–690. [CrossRef]
15. Pan, L.; Ye, S.; Huang, R.; Wang, M.; Lin, P.; Zhang, H.; Wang, D. Luminescence Prop-erties and Theoretical Modeling of the Ag_3 Cluster Confined inside the D6r Cavity of Faujasite Zeolite: Implications for the Design of Tunable Emission Phosphor. *ACS Appl. Nano Mater.* **2024**, *7*, 9934–9941. [CrossRef]
16. Yuan, J.; Li, Q.; Yue, C.; Wang, N.; Li, P.; Li, H. Emission-tunable silver clusters constrained within EMT zeolite. *J. Mater. Chem. C* **2023**, *11*, 17080–17086. [CrossRef]
17. Xv, X.; Ye, S.; Pan, L.; Lin, P.; Liao, H.; Wang, D. Tailoring the Luminescence Properties of Silver Clusters Confined in Faujasite Zeolite through Framework Modification. *Materials* **2022**, *15*, 7431. [CrossRef]
18. Wang, N.; Li, Q.; Yuan, J.; Zhao, D.; Yang, H.; Wang, Y. White light-emitting Ag^+-doped H-SSZ-13 zeolite. *Inorg. Chem. Commun.* **2024**, *168*, 112875. [CrossRef]
19. Tian, X.; Li, Q.; Yao, D.; Li, P.; Li, H.; Wang, Y. Tunable luminescence of silver-exchanged SOD zeolite thermally treated under mild conditions. *J. Mater. Chem. C* **2022**, *10*, 1666–1671. [CrossRef]
20. Zhang, C.; Guan, S.; Li, H.-Y.; Dong, X.-Y.; Zang, S.-Q. Metal clusters confined in chiral zeolitic imidazolate framework for circularly polarized-luminescence inks. *Nano Lett.* **2024**, *24*, 2048–2056. [CrossRef]
21. Haji-Hashemi, H.; Habibi, M.M.; Safarnejad, M.R.; Norouzi, P.; Ganjali, M.R. Label-free electrochemical immunosensor based on electrodeposited Prussian blue and gold nanoparticles for sensitive detection of citrus bacterial canker disease. *Sens. Actuators B Chem.* **2018**, *275*, 61–68. [CrossRef]
22. Liao, H.; Ye, S.; Lin, P.; Pan, L.; Wang, D. In situ growth of lanthanides-doped nanoparticles inside zeolites with enhanced up conversion emission for gallic acid detection. *J. Colloid. Interface Sci.* **2023**, *652*, 1297–1307. [CrossRef] [PubMed]
23. Ma, S.; Li, X.; Yang, Z.; Li, H. Size effect of encapsulated metal within zeolite: Biomass, CO_2 and methane utilization. *J. Catal.* **2023**, *417*, 368–378. [CrossRef]
24. Li, Q.; Tian, X.; Yuan, J.; Zhao, D.; Wang, Y.; Li, H. Tunable luminescence of silver nanoclusters confined in SOD/FAU zeolites and selective sensing for organic amine. *Inorg. Chem.* **2023**, *62*, 2430–2439. [CrossRef] [PubMed]
25. Yuan, X.; Luo, Z.; Yu, Y.; Yao, Q.; Xie, J. Luminescent noble metal nanoclusters as an emerging optical probe for sensor development. *Chem.–Asian J.* **2013**, *8*, 858–871. [CrossRef]
26. De Cremer, G.; Sels, B.F.; Roeffaers, M.B.J.; Coutin, E.; De Vos, D.E.; Vosch, T.; Hofkens, J. Optical encoding of silver zeolite microcarriers. *Adv. Mater.* **2010**, *22*, 957–960. [CrossRef]
27. Yao, D.; Yang, J.; Xie, Y.; Wang, Y.; Wang, Y.; Li, H. Warm white-light phosphor based on a single-phase of $Ag^+/Eu^{3+}/Zn^{2+}$ loading SOD zeolites with application to white LEDs. *J. Alloys Compd.* **2020**, *823*, 153778. [CrossRef]
28. Chakraborty, I.; Pradeep, T. Atomically precise clusters of noble metals: Emerging link between atoms and nanoparticles. *Chem. Rev.* **2017**, *117*, 8208–8271. [CrossRef]
29. Yao, D.; Xu, S.; Wang, Y.; Li, H. White-emitting phosphors with high color-rendering index based on silver cluster-loaded zeolites and their application to near-UV LED-based white LEDs. *Mater. Chem. Front.* **2019**, *3*, 1080–1084. [CrossRef]
30. Baekelant, W.; Aghakhani, S.; Fron, E.; Martin, C.; Woong-Kim, C.; Steele, J.A.; De Baerdemaeker, T.; d'Acapito, F.; Chernysov, D.; van der Auweraer, M.; et al. Luminescent silver–lithium-zeolite phosphors for near-ultraviolet LED applications. *J. Mater. Chem. C* **2019**, *7*, 14366–14374. [CrossRef]
31. Pan, L.; Ye, S.; Xv, X.; Lin, P.; Huang, R.; Wang, D. Zeolite-Encaged Luminescent Silver Nanoclusters. *Materials* **2023**, *16*, 3736. [CrossRef] [PubMed]
32. Shi, Y.; Ye, S.; Liao, H.; Liu, J.; Wang, D. Formation of luminescent silver-clusters and efficient energy transfer to Eu3+ in faujasite NaX zeolite. *J. Solid. State Chem.* **2020**, *285*, 121227. [CrossRef]
33. Coutiño-Gonzalez, E.; Baekelant, W.; Steele, J.A.; Kim, C.W.; Roeffaers, M.B.J.; Hofkens, J. Silver clusters in zeolites: From self-assembly to ground-breaking luminescent properties. *Acc. Chem. Res.* **2017**, *50*, 2353–2361. [CrossRef]
34. *JCPDS# 43-0168*; Zeolite Y, (Na) [Sodium Aluminum Silicate Hydrate]. International Centre for Diffraction Data (ICDD): Newtown Square, PA, USA, 1991.
35. Fenwick, O.; Coutiño-Gonzalez, E.; Richard, F.; Bonacchi, S.; Baekelant, W.; de Vos, D.; Roeffaers, M.B.J.; Hofkens, J.; Samorì, P. X-Ray-Induced Growth Dynamics of Luminescent Silver Clusters in Zeolites. *Small* **2020**, *16*, 2002063. [CrossRef]
36. Yu, J.; Ye, S.; Liao, H.; Xv, X.; Wang, D. Luminescence Control of Silver Nanoclusters by Tailoring Extra-Framework Cations in FAU-Y Zeolite: Implications for Tunable Emission. *ACS Appl. Nano Mater.* **2021**, *4*, 13692–13699. [CrossRef]
37. Price, L.; Leung, K.M.; Sartbaeva, A. Local and average structural changes in zeolite A upon ion exchange. *Magnetochemistry* **2017**, *3*, 42. [CrossRef]

38. Shin, H.S.; Choi, H.C.; Jung, Y.; Kim, S.B.; Song, H.J.; Shin, H.J. Chemical and size effects of nanocomposites of silver and polyvinyl pyrrolidone determined by X-ray photoemission spectroscopy. *Chem. Phys. Lett.* **2004**, *383*, 418–422. [CrossRef]
39. Yang, X.; Liu, Y.; Yan, C.; Chen, G. Solvent-free preparation of hierarchical 4A zeolite monoliths: Role of experimental conditions. *J. Cryst. Growth* **2019**, *528*, 125286. [CrossRef]
40. Altantzis, T.; Coutino-Gonzalez, E.; Baekelant, W.; Martinez, G.T.; Abakumov, A.M.; Van Tendeloo, G.; Roeffaers, M.B.J.; Bals, S.; Hofkens, J. Direct observation of luminescent silver clusters confined in faujasite zeolites. *ACS Nano* **2016**, *10*, 7604–7611. [CrossRef]
41. Yu, J.; Ye, S.; Shi, Y.; Liao, H.; Xv, X.; Wang, D. Confinement of highly luminescent silver nanoclusters in FAUY Zeolite: A study on the formation effects of silver nanoclusters and the sensitization of Tb^{3+}. *ACS Appl. Nano Mater.* **2021**, *4*, 6290–6298. [CrossRef]
42. Yang, J.; Jin, R. Advances in enhancing luminescence of atomically precise Ag nanoclusters. *J. Phys. Chem. C* **2020**, *125*, 2619–2625. [CrossRef]
43. Wang, L.; Zhong, W.; Gao, W.; Liu, W.; Shang, L. Dynamic multicolor luminescent anti-counterfeiting based on spiropyran-engineered gold nanoclusters. *Chem. Eng. J.* **2024**, *479*, 147490. [CrossRef]
44. International Commission on Illumination (CIE). *The CIE 1931 Color Spaces*; CIE Technical Report; CIE: Vienna, Austria, 1931.
45. Ploch, N.L.; Einfeldt, S.; Frentrup, M.; Rass, J.; Wernicke, T.; Knauer, A.; Kueller, V.; Weyers, M.; Kneissl, M. Investigation of the temperature dependent efficiency droop in UV LEDs. *Semicond. Sci. Technol.* **2013**, *28*, 125021. [CrossRef]
46. Ibrahim, M.S.; Jing, Z.; Yung, W.K.; Fan, J. Bayesian based lifetime prediction for high power white LEDs. *Expert. Syst. Appl.* **2021**, *185*, 115627. [CrossRef]

Disclaimer/Publisher's Note: The statements, opinions and data contained in all publications are solely those of the individual author(s) and contributor(s) and not of MDPI and/or the editor(s). MDPI and/or the editor(s) disclaim responsibility for any injury to people or property resulting from any ideas, methods, instructions or products referred to in the content.